# Predissociation of $H_3$ Rydberg states

I. Mistrík, R. Reichle, H. Helm, and U. Müller*

*Fakultät für Physik, Albert-Ludwig-Universität Freiburg, Stefan-Meier-Strasse 19, 79104 Freiburg, Germany*
(Received 13 September 2000; published 20 March 2001)

A fast-beam spectrometer is used to investigate the photofragmentation and autoionization dynamics of laser-excited triatomic hydrogen molecules. The yield of neutral products from rapidly predissociated states of $H_3$ is monitored in parallel with the field ionization signal. Using this spectrometer, we have measured the natural lifetime of low principal quantum number Rydberg states $nsA_1'$ and $npE'$. For the $3sA_1'$, $4sA_1'$, and $5sA_1'$ electronic states, we find lifetimes decreasing with increasing principal quantum number. This is unexpected for a Rydberg series and confirms the observations of a previous investigation. In addition, our experiments give direct evidence that even very high principal quantum number Rydberg states of $H_3$ are selectively subject to strong predissociation. This process appreciably shortens their natural lifetimes. In the high principal quantum number $ns$- and $nd$ Rydberg series converging to the lowest ionization threshold of $H_3$ we find a significant variation of the predissociation yield with principal quantum number and electronic angular momentum. Windows with enhanced predissociation in the Rydberg series are explained by nonadiabatic couplings of the laser-prepared initial states with the repulsive ground states surface mediated by vibrationally degenerate mode excited $4pE'$ and $5pE'$ states. The relevance of the $H_3$ predissociation mechanisms for the dissociative recombination of $H_3^+$ is discussed.

## I. INTRODUCTION

Rydberg states of the triatomic hydrogen molecule can be viewed as an electron attached to a tightly bound $H_3^+$ core [1,2]. These states are embedded in the dissociation continuum of the repulsive electronic ground state surface (Fig. 1). All excited bound states of $H_3$ are subject to predissociation. The metastable $2p^2A_2''$ ($N=K=0$) state is particularly long-lived ($\approx 700$ ns) [3]. Neutral $H_3$ in this state can be prepared in a fast beam and used as a platform for laser-excitation experiments [4–9]. In previous investigations, the dissociation dynamics of state-selected low principal quantum number ($n=2,3$) Rydberg states into $H+H_2$ fragment pairs was investigated [10,11] and rovibrational distributions in the $H_2$ final state were determined. The three-body breakup of $n=3$ Rydberg states of $H_3$ was investigated in kinematically complete experiments, and momentum correlations in the final state distribution were measured [12,13]. High principal quantum number $s$-, $p$-, $d$-, and $f$-Rydberg states were excited by one- and two-color photoexcitation of metastable $H_3$ [14–18]. The rotational, vibrational, and vibronic coupling mechanisms between the Rydberg electron and the ion core were studied theoretically in multichannel quantum defect theory (MQDT) models [17–19].

Previous experiments [3,14,20,21] indicate that predissociation may be effective at even high principal quantum numbers which significantly affects the natural lifetime of these states. It is suspected that such states play an important role in the dissociative recombination (DR) of $H_3^+$ ions with electrons. The absolute DR cross section of $H_3^+$ was measured by Larsson *et al.* [22] and Datz *et al.* [23]. At low electron energy, the measured cross section is approximately four orders of magnitude higher than current theory which only includes the direct DR process predicts [24]. Additional resonant channels via interlopers built on vibrationally excited $H_3^+$ cores which predissociate by coupling to the electronic ground state have been invoked [25] as origin for the huge increase of the DR cross section at low energy. Vibrational couplings play an important role in the DR of light molecules [26–28]. However, the predissociation mechanisms of high principal quantum number Rydberg states of $H_3$ in the vicinity of the lowest ionization threshold are not yet understood.

To investigate the photodissociation dynamics of laser-excited neutral molecules, we have added a detector for neutral fragments in off-axis geometry to the Freiburg photoionization spectrometer [29,30]. This enables us to directly observe photofragments from laser-prepared high principal quantum number Rydberg states of $H_3$ while at the same time monitoring autoionizing states. Pronounced modulations in the photofragment yield of the $s$- and $d$-Rydberg members appear, revealing yet unknown coupling structure of bound and continuum states in the reference frame of Fig. 1.

## II. LABELING OF THE $H_3$ STATES

To label the rotational and vibrational levels of the $H_3$ Rydberg states, we use the notation $(N,K,G)\{\nu_1,\nu_2^{l_2}\}$ with the total angular momentum $N$ apart from electron spin, the projection of $N$ on the molecular top axis $K$, and Hougen's convenient quantum number $G$ [31]. The vibrations are classified by the quantum numbers of the symmetric stretch ($\nu_1$) and the degenerate mode ($\nu_2$) and by the vibrational angular momentum $l_2$. Although $K$ is not a good quantum number in states with electronic angular momentum $l>0$ and/or vibrational angular momentum $l_2>0$, we retain it for easier comparison with previous publications [18]. To label states of the

---

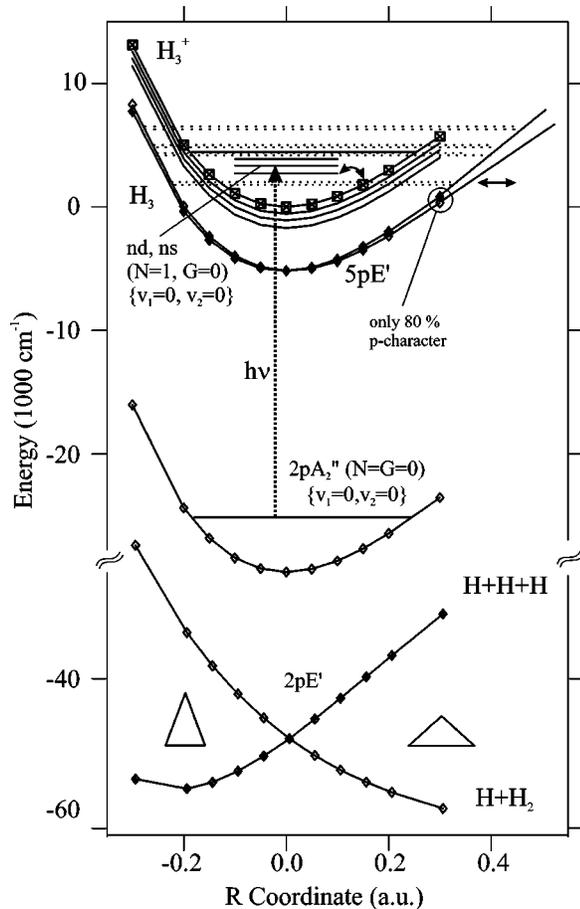*Electronic mail address: Ulrich.Mueller@uni-freiburg.de

FIG. 1. Cut through the potential energy surfaces of the $H_3$ states relevant for this paper. The symbols show the energies of the $H_3^+$ ion ⊠ and of the $2p^2E'$, $2p^2A_2''$, and $5pE'$ states of $H_3$ ( ◇ ) calculated by *ab initio* quantum chemical methods [18]. The selected points follow the $R$ coordinate for $S=0$ and correspond to a set of equilateral geometries [see Fig. 1(b) in Ref. [18]].

$H_3^+$ ion, a superscript $^+$ is added to the quantum numbers. A cut through the potential energy surfaces of $H_3$ and the levels relevant for this paper are shown in Fig. 1. The $2p^2A_2''$ $(0,0,0)\{0,0^0\}$ state in it's lowest rotational level is metastable. From this state, we can photoexcite states with an angular momentum $N=1$, $G=0,3$ and an overall symmetry $A_2'$ in single photon excitation. We expect to preferentially

observe vibrationless $ns$- and $nd$-Rydberg series, strongly favored by Franck-Condon factors. In vibrationally nondiagonal transitions, $ns$, $nd$, and $np$ states with several quanta in the degenerate vibrational mode can also be excited.

## III. EXPERIMENT

A schematic of the experimental setup is shown in Fig. 2. The preparation of the metastable beam is similar to that in previous investigations [4,17,18]. $H_3^+$ ions are created in a hollow cathode discharge source ($I$), accelerated to a kinetic energy of 3.6 keV (ACC), mass selected in a Wien filter (WF), and neutralized by charge transfer in cesium (CT). After the charge transfer cell, residual ions and $H_3$ molecules in high principal quantum number Rydberg states are removed by an electric field (ID). The beam of fast $H_3$ molecules in the metastable $2p^2A_2''$ state enters the differentially pumped interaction region through an aperture ($A$) of 1.6 mm diameter. The pressure in the interaction chamber is kept below $5\times10^{-9}$ mbar to minimize the amount of dissociation processes induced by restgas collisions. The $H_3$ metastable beam is merged coaxially with the beam of a pulsed dye laser pumped by an excimer laser. Neutral fragments produced in predissociation of laser-excited $H_3$ separate from the fast parent beam due to the kinetic energy release in the center of mass frame. They are detected on a set of microchannel plates (MCP1) with 40 mm diameter in a distance of 90 cm from the aperture ($A$). Fragments arriving in a 0.5 $\mu$s wide time interval starting 1.2 $\mu$s after each laser shot are counted.

The $H_3$ states investigated in this paper may decay by two-body predissociation into $H + H_2X^1\Sigma_g^+(v,J)$, by three-body decay into $H(1s)+H(1s)+H(1s)$, and by photoemission into lower electronic states followed by two- or three-body breakup. Two-body predissociation leads to kinetic energies in the 3.1 to 9.3 eV range. Three-body predissociation appears with a total kinetic energy between 3.1 and 4.8 eV. Radiative transitions to the $2p^2E'$ ground state surface with subsequent two-body decay produce a continuous kinetic energy distribution between 0.5 and 4.5 eV peaking at about 2.5 eV [10,11,32,33]. The metastable state itself slowly decays into $H+H_2$ with a similar continuum in the kinetic energy release spectrum [11]. The fragment detection
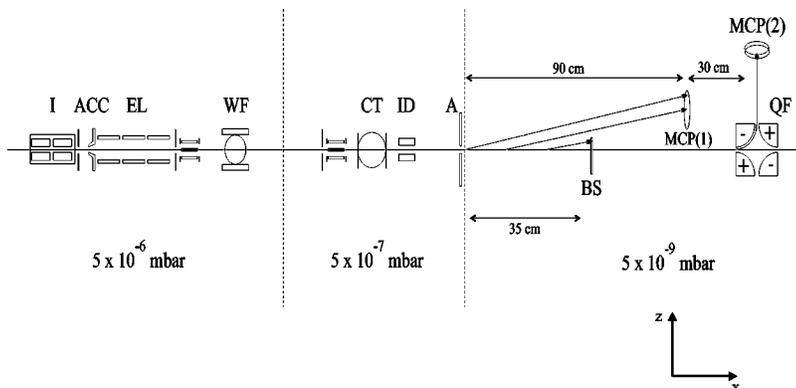


FIG. 2. Schematics of the Freiburg photoionization/fragmentation spectrometer. Legend: $I$ (ion source), ACC (acceleration), EL (lens), WF (Wien filter), CT (charge transfer cell), ID (ion deflector), $A$ (differential aperture), BS (optically transparent stop for metastable beam), MCP1 (detector for neutral fragments), MCP2 (ion detector), QF (quadrupole energy analyzer).

efficiency is a function of their angular distribution and their radial separation from the parent neutral beam path. It depends on the laser polarization and the branching between the decay processes. In our apparatus, the lateral separation of the fragment detector from the fast beam ($x$) axis can be varied. This allows us to preferentially detect fragments from predissociation and to discriminate against contributions from the parent metastable beam and the radiative decay. For the investigations in this paper, we found an optimum signal to background ratio at a separation between the $x$ axis and the edge of the detector of 2.5 cm. The lateral displacement of the detector from the neutral beam axis defines a reference axis ($z$ axis) in the laboratory frame. We can record spectra with the polarization of the excitation laser parallel or perpendicular to the $z$ axis. An alignment of the fragment ejection with respect to the electric field of the laser gives further insight into the symmetry of the excited state or into the fragmentation mechanism. To further reduce the background of neutral products from metastable decay, the parent beam can optionally be intercepted by a transparent beam stop (BS) in the form of a quartz plate. This beam stop is mounted on a mechanical feedthrough at a distance of 35 cm from the aperture ($A$). However, the background in the spectra shown in this paper is extremely low, even without the beam stop. In the absence of the beam stop, $H_3$ molecules which survive the 2 $\mu$s flight time to the quadrupole (QF) can be field ionized, energy selected, and counted by a second detector (MCP2). This detector also allows us to monitor autoionization [17,18,29,30].

The laser frequency was calibrated using atomic lines of argon. Corrections for the refraction index of air and for the Doppler shift due to the velocity of the neutral beam were applied.

## IV. EXPERIMENTAL RESULTS

### A. Lifetimes of low principal quantum number Rydberg states

Predissociation spectra of the $3s$, $4s$, and $5s$ states are shown in Fig. 3. To reduce power broadening, the laser intensity was limited such that the height of the peaks was about 30% of the saturation. The linewidth of the transitions was obtained by fitting a Lorentzian to the measured curves. We have subtracted the instrumental linewidth ($\gamma_l = 0.05$ cm$^{-1}$ with intracavity etalon, $\gamma_l = 0.15$ cm$^{-1}$ without etalon) from the fitted values and corrected the residual saturation broadening [34]. The fitted and the corrected values are listed in Table I and compared with the results of previous measurements [9,20].

The line shape of the transition to the vibrationless $4sA_1'$ state is fitted very well by a Lorentzian. The $5sA_1'$ line is slightly asymmetric which might be due to a coupling with a perturber. We have fitted the $5s$ line by a double Lorentzian profile and listed both components in Table I. The linewidths of the $s$-states measured by us are in excellent agreement with those determined previously in depletion spectroscopy [9].
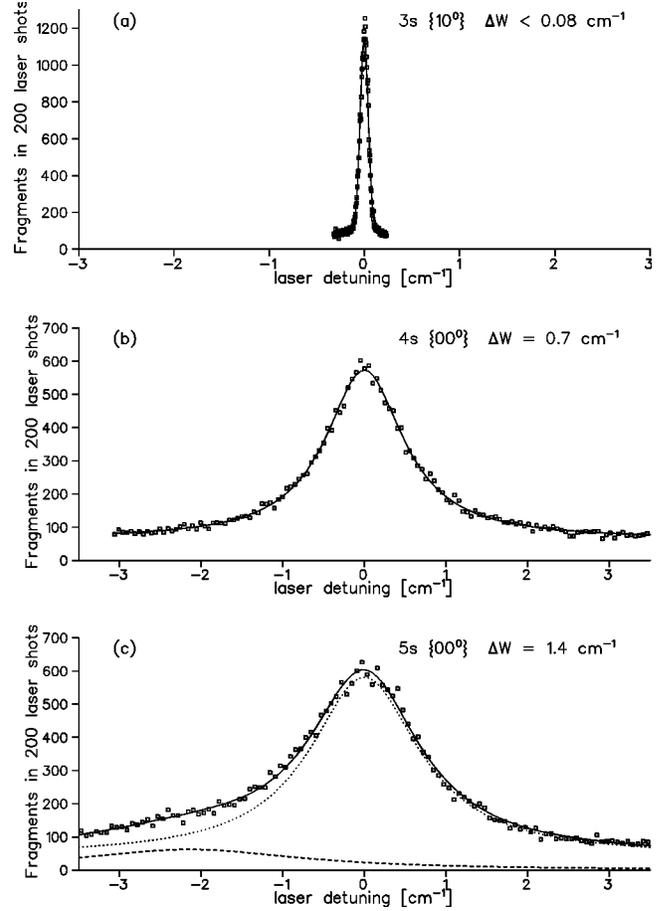


FIG. 3. Predissociation spectra of the low principal quantum number Rydberg states $3sA_1'\{10^0\}$ [(a)], $4sA_1'\{00^0\}$ [(b)], and $5sA_1'\{00^0\}$ [(c)] of $H_3$. The fitted Lorentzian line shapes are shown as solid lines. The fitting of $5s$ required two components shown by the dashed lines.

### B. Predissociation of high principal quantum number $s$- and $d$-Rydberg states

High principal quantum number Rydberg states ($n \geqslant 30$) can be investigated by monitoring both the field ionization signal and the photofragment yield. In Fig. 4 the photofragment yield [(a),(b)], as well as the field ionization signal (c) are shown following photoexcitation of the $H_3$ $2p^2A_2''(0,0,0)\{0,0^0\}$ state in the spectral range 29 480 to 29 580 cm$^{-1}$. Spectra (a) and (b) were recorded with the laser polarization perpendicular and parallel to the $z$ axis, respectively. The field ionization spectrum (c) in Fig. 4 closely agrees with that observed in previous investigations [4–6,14]. The transitions in the ionization spectrum were assigned to the $d$-Rydberg series converging to the $H_3^+(1,0,0)\{0,0^0\}$ threshold [5]. This threshold lies at 29 562.14 cm$^{-1}$ [7] and is marked by a dashed line in Fig. 4. Up to the highest resolved principal quantum numbers, we find contributions to the photofragment signal. This shows that the Rydberg states predissociate noticeably on a time scale of about 2 $\mu$s. Note that no signal increase is observed on the photodissociation detector above the ionization threshold. This shows that neither photoions nor photoelec-

TABLE I. Linewidths and lifetimes of low principal quantum number Rydberg states of $H_3$.

| State[a] | This work $h\nu$[b] | linewidth (cm$^{-1}$) fitted | linewidth (cm$^{-1}$) corrected | Lifetime $\tau$ | Previous expt. linewidth (cm$^{-1}$) | Previous expt. Lifetime | Theory Calc. lifetimes radiat.[c] | Theory Calc. lifetimes prediss.[d] |
|---|---|---|---|---|---|---|---|---|
| $2sA_1'\{00^0\}$ | $-898$[e] | | | | 30 | 190 fs[e] | 32 ns | 1.7 ps |
| $3sA_1'\{00^0\}$ | 16694.992[f] | | | | $\leq 0.007$[f] | $\approx 1$ ns[g] | 75 ns | 8 ns |
| $3sA_1'\{10^0\}$ | $19907.1 \pm 0.3$ | 0.1 | $<0.08$ | $>66$ ps | | | 75 ns | 1.4 ns |
| $4sA_1'\{00^0\}$ | $22422.2 \pm 1$ | 0.9 | $0.7 \pm 0.15$ | 7.6 ps | 0.7[h] | 7.6 ps[h] | 200 ns | |
| $5sA_1'\{00^0\}$ | $25032.2 \pm 1$ | 1.63 | $1.4 \pm 0.15$ | 3.8 ps | 1.2[h] | 4.4 ps[h] | | |
| | $25030.1 \pm 1$ | 3.3 | $2.8 \pm 0.15$ | 1.9 ps | | | | |
| $3pE'\{01^1\}$ | $15548.8 \pm 1$ | 0.08 | $<0.08$ | $>66$ ps | | | 21 ns | 39 ps[i] |
| $4pE'\{01^1\}$ | $23805.8 \pm 0.2$ | 0.31 | $0.25 \pm 0.05$ | 21 ps | | | 54 ns | |
| $6dE''\ N=1\ \{10^0\}$[j] | $29674 \pm 2$ | $\approx 2.7$ | | $\approx 2$ ps | | | | |
| $5pA_2''\ N=2\ \{02^2\}$[j] | $13144 \pm 1$ | $\approx 0.9$ | | $\approx 6$ ps | | | | |
| $20pE'\ N=2\ \{10^0\}$[j] | $12548.5 \pm 1$ | $\approx 1$ | | $\approx 5$ ps | | | | |

[a]Rotational state ($N=1, G=0$).
[b]Energy relative to $2p^2A_2''$ (0,0,0)$\{0,0^0\}$ in cm$^{-1}$.
[c]Radiative lifetime calculated from *ab initio* dipole transiton moments for optical dipole transitions [36].
[d]From the sum of the two- and three-body predissociation rates calculated by Schneider and Orel [25].
[e]From Herzberg's data [2].
[f]Bjerre *et al.* [20].
[g]This value results from the observation of a lower limit $\tau > 750$ *ps* of Ref. [20] and an upper limit of $\tau < 3$ ns of Ref. [39].
[h]From the linewidths of Ref. [9].
[i]Values of the $3pE'$ vibrational ground state.
[j]For these states, the rate of predissociation is of the same order of magnitude as autoionization.

trons produced by direct ionization of $H_3$ reach the off-axis detector. The windows in the field ionization intensity close to $n=44$ and $n=61$ correlate with enhanced fragment yield. This confirms previous laser depletion experiments [14] and shows that the intensity modulations are caused by a shortening of the lifetime due to predissociation. The effect is

most clearly visible in the spectrum with laser polarization parallel to the $z$-axis Fig. 4(b). With perpendicular laser polarization, the photodissociation signal in the vicinity of $n = 44$ is significantly larger than that at $n = 61$. This suggests that the doorway states mediating the predissociation process are different in nature at $n=44$ and $n=61$. Bordas and Helm
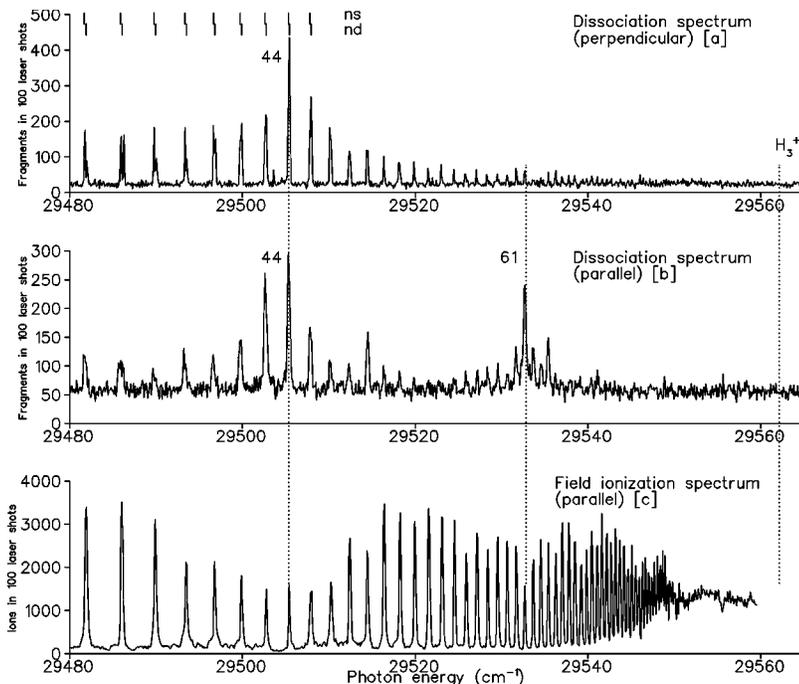


FIG. 4. Laser excitation of $H_3$ in the vicinity of the lowest ionic limit. Comparison of the photofragment yield (a),(b) and the field ionization spectrum (c). In (a), the laser polarization was perpendicular, in (b) parallel to the axis defined by the lateral displacement of detector for neutral fragments. The $ns$- and $nd$-Rydberg series converging to the $H_3^+$ (1,0)$\{0,0^0\}$ threshold are indicated by tickmarks.
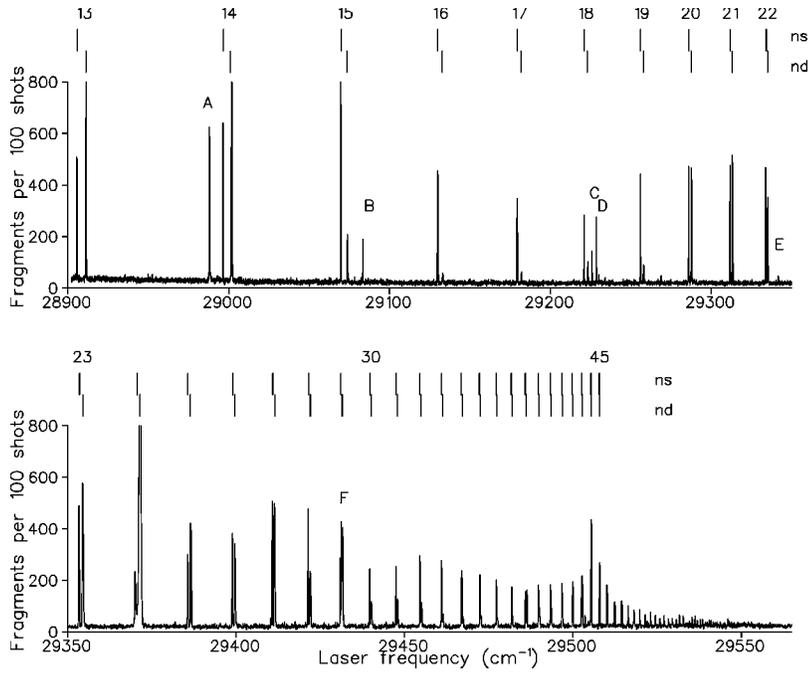
FIG. 5. Spectrum of the photofragment yield in the 28 900 to 29 570 cm$^{-1}$ energy range above the $2p^2A_2''(0,0)\{0,0^0\}$ state of H$_3$. The laser polarization was perpendicular to the detector axis. The $ns$- and $nd$-Rydberg series converging to the H$_3^+$ (1,0)$\{0,0^0\}$ threshold are indicated by tickmarks. Interlopers are labeled by A–F.

[14] found a pronounced electric field dependence of the intensity window at $n=61$ and attributed this to Stark mixing with the $npE'$ series. The predissociation around $n=44$ was found not to be sensitive to external electrical fields.

In the spectra of the photofragment yield, in addition to the $nd$-Rydberg series, $s$ lines converging to the H$_3^+$(1,0,0)$\{0,0^0\}$ threshold are observed. The $ns$ lines absent in the ionization signal appear most prominent in the low-energy region of the spectrum Fig. 4(a) where they separate from the $d$ lines. The photofragment detector allows us to follow the Rydberg series to low principal quantum numbers well below our field ionization limit at $n\approx31$. The spectrum of the photofragment signal starting from principal quantum number $n=13$ to the ionization threshold is shown in Fig. 5. We observe characteristic intensity modulations in the $ns$- as well as the $nd$-Rydberg series. In addition to the already known interlopers at $n=44$ and $n=61$, we find increased predissociation close to $n=14$ and $n=21$. We have fitted the line positions with a Rydberg formula

$$h\nu = E_{\lim} - R/(n-\delta)^2. \qquad (4.1)$$

With the Rydberg constant $R=109717.40$ cm$^{-1}$ for H$_3$, we find the quantum defects $\delta_s = 0.072 \pm 0.002$ for the $ns$ and $\delta_d = 0.012 \pm 0.001$ for the $nd$ series. The quantum defects are slightly smaller than those observed in the deuterated isotopomer [29]. Our fitted value of the H$_3^+$(1,0,0)$\{0,0^0\}$ threshold $E_{\lim} = 29562.15 \pm 0.1$ cm$^{-1}$ is in excellent agreement with the value of Ketterle *et al.* 29562.14$\pm$0.1 cm$^{-1}$ [7]. The $s$ and $d$ series in the spectrum are marked by ticks in Fig. 5. Most members of the $ns$ and $nd$ series are in agreement with the Rydberg formula to within 0.2 cm$^{-1}$. However, perturbations which shift the line positions by more than 0.5 cm$^{-1}$ appear at 13$d$, 14$d$, and 24$s$.
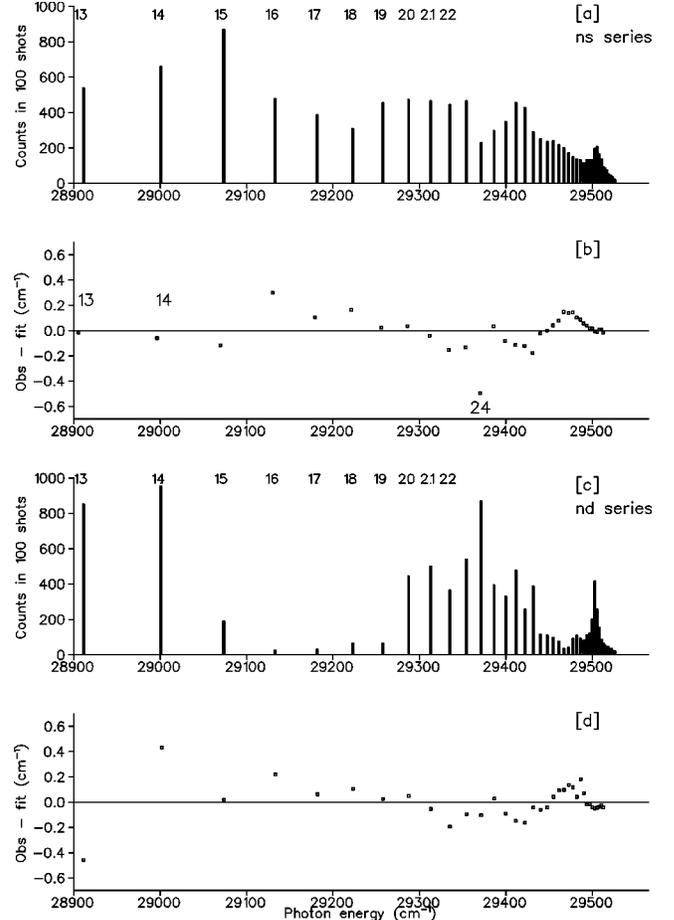


FIG. 6. Perturbations in the $ns$ and $nd$ series of H$_3$. The line intensities for predissociation are indicated by solid bars. The difference between the observed line position and that calculated by the Rydberg formula are shown by the squares.

TABLE II. Rovibronic interlopers appearing in the photofragment yield spectrum of $H_3$.

| Label | $h\nu_{exp}$[a] | Core state[b] | Core energy[c] | $\nu$[d] | Electronic state |
|-------|-----------------|---------------|----------------|----------|------------------|
| A | 28988.1 | $(1,1,0)\{0,1^1\}$ | 2616.6567 | 5.945 | $6pA_2''$ |
| B | 29083.3 | $(3,0,0)\{0,0^0\}$ | 516.9207 | 10.988 | $11d(E''$ and $A_1')$ |
| C | 29225.9 | | | | |
| D | 29228.5 | $(3,0,0)\{0,0^0\}$ | 516.9207 | 11.987 | $12d(E''$ and $A_1')$ |
| E | 29341.6 | $(3,0,0)\{0,0^0\}$ | 516.9207 | 12.987 | $13d(E''$ and $A_1')$ |
| F | 29431.2 | $(3,0,0)\{0,0^0\}$ | 516.9207 | 13.986 | $14d(E''$ and $A_1')$ |

[a]Energy in $cm^{-1}$ above $H_3 2p^2 A_2''(0,0,0)\{0,0^0\}$. The experimental uncertainty is $\pm 0.2$ $cm^{-1}$.

[b]$H_3^+$ states labeled by quantum numbers $(N^+,K^+,G)\{\nu_1\nu_2^{l_2}\}$.

[c]Energies of $H_3^+$ in $cm^{-1}$ from Ref. [35] relative to the $N^+=0$ ground state. The energy of the lowest *ortho* state $(1,0,0)\{0,0^0\}$ is 86.9683 $cm^{-1}$.

[d]Effective principal quantum number determined from the core energy and the 29562.15 $cm^{-1}$ energy of the $H_3^+(1,0,0)\{0,0^0\}$ state above $H_3 2p^2 A_2''(N=K=0)\{0,0^0\}$.

To locate perturbations in the $nd$ and $ns$ series, we have plotted in Fig. 6 the intensities of the lines up to $n=50$. The $s$ and $d$ series intensities both assume minima in the vicinity of $n=17$ and $n=40$ and maxima near $n=14$ and $n=44$. An exception occurs at $n=24$, where the $d$ series shows a maximum and the $s$ series a minimum. The modulations in the $s$ series are more prominent than those in the $d$ series.

Several interloper states which are attributed to Rydberg molecules built on higher rovibrationally excited ionic cores appear in the spectrum. They are labeled by A–F in Fig. 5 and listed in Table II. The assignment is based on the symmetry properties of the Rydberg states [8]. The ionic limits from which the effective principal quantum numbers are derived are taken from Ref. [35]. Lines B, D, E, and F are members of the $nd(A_1',E'')$ series built on a $H_3^+(3,0,0)\{0,0^0\}$ core. They converge to an ionization threshold at $E_{lim}=30014.95$ $cm^{-1}$ and show an almost constant quantum defect of $\delta_{d3}=0.013$. In contrast to the $p$ series [17,18], the $d$ series built on $N^+=1$ and $N^+=3$ cores show no effect of rotational coupling. This confirms that the $d$ states of $H_3$ are very close to pure Hund's case $d$ coupling [15]. Because of the smaller transition dipole moment, the intensity of the series converging to the $(N^+=3,G=0)$ ionic limit is lower than that of the series built on a $(N^+=1,G=0)$ core. The strong resonance A at 28988.1 $cm^{-1}$ is particularly interesting. We assign this line to the $6pA_2''$ state converging to the bending excited ionic limit $(1,1,0)\{0,1^1\}$ with a quantum defect of $\delta=0.055$. This assignment is based on the observation of the corresponding $3pA_2''$ and $4pA_2''$ states [8] with nearly the same quantum defect and the good agreement with the results of *ab initio* quantum chemical calculations [18].

### C. Predissociation above the first ionization threshold of $H_3$

In previous investigations from this laboratory [17,18], we have found indications that autoionizing $H_3$ Rydberg states above the first ionization threshold may be subject to appreciable predissociation. In the $np$ series built on a symmetric-stretch excited $H_3^+$ core, the positions, relative amplitudes, and widths of most of the quasidiscrete lines

were understood by a MQDT calculation. However, for a few members of the series, the measured relative intensities were lower and the line widths were broader than those predicted. This observation may indicate predissociation competing with autoionization. As an example, we have measured the spectrum of the photofragment yield in the vicinity of the $20p \{1,0^0\}$ states excited via the $3sA_1'(1,0,0)\{1,0^0\}$ intermediate. The autoionization and predissociation spectra in the 12 542 to 12 548 $cm^{-1}$ spectral range (369.46 to 370.20 meV above the ionization threshold) are shown in Figs. 7(e) and 7(f), respectively. The dotted line in Fig. 7(e) gives the prediction of the MQDT calculation from Ref. [18]. In such a two-photon measurement, a significant background of neutral products originates from predissociation of the intermediate state. To reduce this background the polarization of the first laser was chosen parallel and that of the second laser perpendicular to the orientation of the off-axis detector. This allows us to pump states with total angular momentum $N=1$ and $N=2$ [16–18]. In the dissociation spectrum, the constant background was subtracted. A peak appears in the spectrum of the neutral fragments which corresponds to the state with total angular momentum $N=2$. The small dip observed at the position of the state with total angular momentum $N=1$ (12 546.2 $cm^{-1}$) is due to depletion of the intermediate state. In Fig. 7(f), the photofragment count rate was normalized to the maximum of the photoion rate. Taking into account the geometric collection efficiency of the off-axis detector which we estimate by a Monte Carlo simulation to be smaller than 12%, we find that the branching between predissociation and autoionization of the $N=2$ state is higher than 25%. Apparently, the $N=2$ state is strongly predissociated while the decay of the $N=1$ state is dominated by autoionization.

As an example for a $d$ state, we have investigated the symmetric-stretch excited $6dE''(1,1,0)\{1,0^0\}$ state of $H_3$ which can be excited from the $2p^2 A_2''(0,0,0)\{0,0^0\}$ state in a Franck-Condon nondiagonal transition. The autoionization and predissociation spectra are also shown in Figs. 7(a) and 7(b). The Fano-type shape of the line profile is caused by the interference with the underlying ionization continuum. If we assume that the collection efficiency of the fragment detector
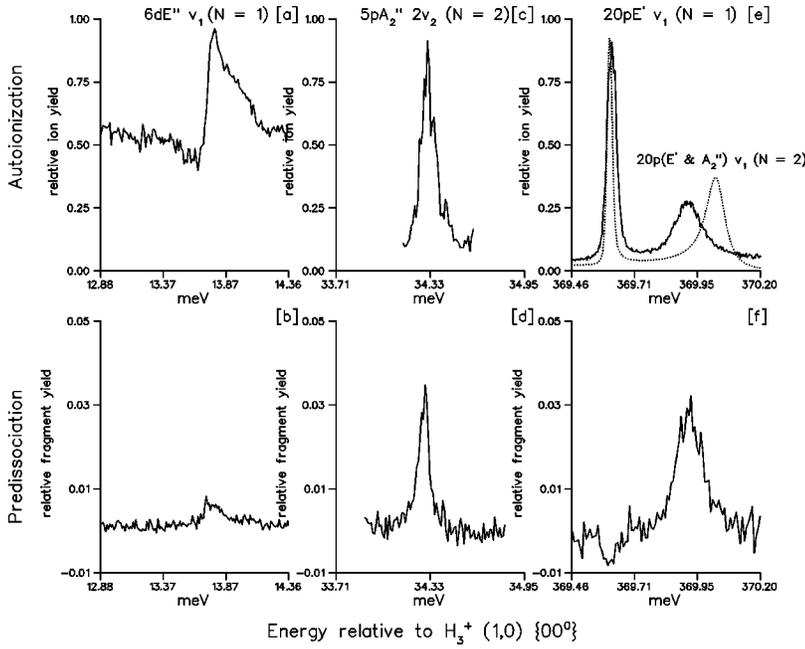
FIG. 7. Enhanced predissociation competing with autoionization above the first ionization threshold of H$_3$. The dotted curve gives the prediction of the MQDT theory of Ref. [18].

does not depend on the principal quantum number of the initial state, the dissociation spectra of the $20pE'/A_2''$ and the $6dE''$ states can be compared on a relative intensity scale. We find that the decay of the $6dE''$ state is dominated by autoionization and that predissociation of this state plays only a minor role.

A third state where predissociation competes with autoionization is the $5pA_2''(2,1,0)\{0,2^0\}$ level shown in Figs. 7(c) and 7(d). As evident from the energy scale, low energy electrons will find such states in the collision continuum and thereby find access to the neutral ground state continuum.

## V. DISCUSSION OF THE PREDISSOCIATION MECHANISMS OF H$_3$

In the absence of predissociation, the only decay routes of the H$_3$ Rydberg states below the first ionization threshold are radiative processes. The radiative rates can be estimated from the *ab initio* transition dipole moments calculated by King and Morokuma [36]. For states which are known to predissociate very weakly, e.g., the $3dE''$ state in D$_3$, the lifetimes estimated from the *ab initio* radiative transition moments are close to the observation [33]. In Table I, we have listed the calculated radiative lifetimes for the states up to $n=4$. These values fall in the nanosecond range, several orders of magnitude longer than the measured values. The photoemission rates for higher principal quantum numbers are expected to scale with $n^{-3}$. Consequently, radiative transitions play a minor role in the decay processes of the states investigated in this paper.

The main decay route of H$_3$ Rydberg states below the first ionization threshold is predissociation as discussed theoretically in several publications [25,37]. The potential energy surfaces of the H$_3$ Rydberg states parallel the surface of the H$_3^+$ ion. No avoided crossings with the repulsive $2p^2E'$ ground states surface are accessible in the vicinity of the equilibrium geometry. Recent *ab initio* calculations [18] of

the geometry-dependent *p*-state quantum defects for $n=3,4,5$ show that even the *p*-Rydberg state potential energy surfaces do not touch the ground state surfaces. Only in linear geometry the calculations by Petsalakis *et al.* [38] indicate a series of avoided crossings between the upper sheet of the ground states surface and all Rydberg states of $\Sigma_g^+$ symmetry. The predissociation of H$_3$ is believed to be caused by a breakdown of the Born-Oppenheimer approximation [25]. The motion of the nuclei induces a coupling between the adiabatic Born-Oppenheimer states. In the $D_{3h}$ equilibrium geometry, the electronic symmetry of the ground state surface is $E'$. The *p* states with $A_2''$ and the *d* states with $E''$ electronic symmetry are predissociated by the tumbling rotation ($E''$ symmetry) about the axis perpendicular to the top axis. Therefore, the members of the *d*-Rydberg series with low rotational excitation ($N=1$) converging to the lowest ionization threshold show comparatively long lifetimes. The linewidths of the low principal quantum number *d* states are much smaller than the bandwidth of our laser. The high principal quantum number *d* states survive the travel time (about 2 $\mu$s) to the field ionization detector. The *s* states which have $A_1'$ electronic symmetry acquire an $E'$ component by the degenerate mode vibration which is always present in the zero point oscillation. This coupling appreciably shortens the lifetime of all *s* states regardless of their rotational excitation. Even high principal quantum number *s*-states decay appreciably during the travel time in the interaction region. They can be observed preferentially in the fragmentation spectra. In the case of D$_3$, the predissociation is much slower due to the higher mass of the nuclei, and both *s* as well as *d* series were observed [29,30] in field ionization. The predissociation of $pE'$ states is not restricted by symmetry and limited solely by the magnitude of the coupling matrix elements.

### A. Low principal quantum number Rydberg states of H$_3$

Schneider and Orel [25] have theoretically investigated the predissociation of the $2s^2A_1'$, $3p^2E'$, and $3s^2A_1'$ states

of $H_3$ and $D_3$ by a two-dimensional wave packet method which explicitly includes the nonadiabatic couplings induced by the vibrational motion of the nuclei. In Table I, we have listed the lifetimes calculated from the sum of the theoretical two- and three-body predissociation rates by Schneider and Orel [25]. These values agree with the experimental data for $n=3$ within about an order of magnitude. For higher principal quantum number states, we would expect an increase in lifetime due to the reduced coupling strength between the Rydberg electron and the core. Therefore, the observed reduction in lifetime with increasing principal quantum number from $n=3$ to $n=5$ of the $s$ states is very surprising. We see a similar trend in the lifetime of the $pE'$ states. Apparently, the $n=4,5$ states are subject to additional coupling mechanisms with the repulsive ground state surface. Such processes may be due to avoided crossing between the excited state potential energy surfaces and the $2p^2E'$ surface, or by nonadiabatic couplings induced by the rotational, and vibrational motion of the core. Since not only the $s$ but also $p$ states are affected, we believe that the couplings are induced by nonadiabatic interactions. For a clarification of the predissociation mechanisms of the $n=4$ and $n=5$ states of $H_3$, detailed *ab initio* theoretical investigations of the nonadiabatic coupling matrix elements are required.

### B. High principal quantum number Rydberg states of $H_3$

We attribute the localized intensity modulations close to $n=14$, $n=24$, $n=44$, and $n=61$ in the high principal quantum number $s$- and $d$-Rydberg spectra to interaction with highly vibrationally excited doorway states which are themselves rapidly predissociated. They open additional decay routes enhancing the photofragment signal. The coupling, however, is weak and deviations of the transition frequencies from the Rydberg formula are barely visible (see Fig. 6). The perturber location does not follow the typical pattern of a Rydberg series. Therefore, we suspect isolated low principal quantum number electronic states in high rovibrational levels. If the perturbation is not induced by the Stark effect due to motional electric fields from uncompensated residual magnetic fields [14], parity and total angular momentum are conserved. We are searching for perturbers with $N=1$ and an overall symmetry $A_2'$. They can interact with $s$ as well as $d$ states. The modulations appear more prominent in the $d$ series which is rotationally predissociated and lives longer than the vibrationally predissociated $s$ series. Possible candidates are electronic $s$, $p$, and $d$ states (angular momentum $L=0,1,2$, respectively) combined with $H_3^+$ cores with angular momentum $N^+$ in the range $|L-N|\leqslant N^+\leqslant|L+N|$. The overall symmetry of the cores has to be $A_2'$ for $s$ and $d$ electrons and $A_2''$ for $p$ electrons [8]. Because we start with an ortho state of $H_3$ ($G=0$), the quantum number $G$ of the core states has to be zero or an integer multiple of 3. These criteria leave only a limited number of $H_3^+$ rovibrational states as possible cores to the doorway states. Their energies are precisely known from recent *ab initio* calculations by Polyansky and Tennyson [35].

For these core states, we determine the effective quantum numbers $\nu$ and quantum defects $\delta$ for the perturber positions

close to $n=14,24,44$, and $n=61$. Electronic states with $n\geqslant6$ can be excluded as perturbers by energy considerations. In addition, we excluded long-lived states with $n=3$. To further reduce the number of possible combinations, we require the quantum defects to be compatible with typical values in Hund's case (b) coupling: $\delta=0.05\cdots0.08$ for $sA_1'$, $\delta\lesssim0.017$ for $dE''$, $\delta=0.03\cdots0.07$ for $dE'$, $\delta=0.36\cdots0.42$ for $pE'$, and $\delta=0.03\cdots0.075$ for $pA_2''$ states. The combinations which meet these criteria are listed in Table III. It seems very unlikely that the $pA_2''$ and $dE''$ states which themselves are weakly predissociated by rotational coupling can be held responsible for the perturbations. The $4pE'$ and $5pE'$ states which have the same electronic symmetry as the ground states are much more likely candidates. The feature at $14d$ correlates with the $4pE'$ state combined with a core having symmetric stretch as well as degenerate mode excitation $\{1,2^2\}$. The intensity modulation close to $24d$ is most probably due to the $5pE'$ state combined with a core having two quanta of excitation in the degenerate vibrational mode $\{0,2^2\}$. The resonances at $44d$ and $61d$ both can be explained by either $4pE'$ with a $\{2,1^1\}$ or $5pE'$ with a $\{0,2^2\}$ core. They might be two Jahn-Teller components of the same electronic state. This could explain their different behavior under the influence of an external electric field as observed by Bordas and Helm [14].

To visualize the proposed dissociation mechanism, cuts through the potential energy surfaces of $H_3^+$ and the $2p$ and $5p$ surfaces of $H_3$ are shown in Fig. 1. The points in Fig. 1 are results of recent *ab initio* quantum chemical calculations [18] shown for a set of equilateral ($C_{2v}$) geometries along the $R$ coordinate with $S=0$ [see Fig. 1(b) in Ref. [18]]. The laser-excited high principal quantum number $s$- and $d$-states are supported by potential surfaces which parallel the $H_3^+$ surface. The doorway states indicated by the horizontal dashed lines in Fig. 1 mix with energetically close $d$ states. The perturbers with $4pE'$ and $5pE'$ electronic symmetry are built on cores which carry one or two quanta of excitation in the degenerate vibrational mode. This allows asymmetric deformations of the nuclear geometry away from the equilibrium. For such geometries, strong $l$ mixing of the $3p$-, $4p$-, as well as $5p$-quantum defect surfaces was found in recent *ab initio* calculations [18] which may favor coupling with the $s$ and $d$ states. The marked point of the $5pE'$ surface in Fig. 1 (geometry point 12 in Ref. [18]) shows only 80% $p$ character. The $4p$ and $5p$ states are known to dissociate rapidly by nonadiabatic coupling to the $2p^2E'$ ground state surface as discussed in Sec. V A.

To finally determine the coupling process which shortens the lifetime of the states, experimental and theoretical data on rovibrationally excited $4pE'$ and $5pE'$ states would be helpful. Two- and three-step laser-excitation schemes to pump such states have now become feasible with our new apparatus. In addition, an extensive theoretical investigation of nuclear geometries far away from equilibrium, and an analysis of the Jahn-Teller coupling of vibrationally excited $npE'$ states is needed.

### C. Relevance to dissociative recombination

The predissociation of $H_3$ Rydberg states plays an important role in the understanding of the dissociative recombina-

TABLE III. Interloper resonances enhancing the predissociation of the $nd$ states of $H_3$. The states with comment $-$ are not likely to be the doorway states which mediate predissociation.

| Perturber near | $h\nu$[a] | $H_3^+$[b] core | $\Gamma_c$ | $H_3^+$[c] energy | $\nu$[d] | $\delta$[e] | Electronic state | Comment |
|---|---|---|---|---|---|---|---|---|
| $14d$ | 29002 | $(2,2,3)\{0,1^1\}$ | $A_2'$ | 2614.2276 | 5.961 | 0.039 | $6dE'$ | $-$ |
| | | $(1,0,0)\{0,1^1\}$ | $A_2''$ | 2616.6567 | 5.959 | 0.041 | $6pA_2''$ | $-$ |
| | | $(1,1,3)\{1,2^2\}$ | $A_2''$ | 7872.1364 | 3.626 | 0.374 | $4pE'$ | $+$ |
| | | $(2,1,3)\{1,2^2\}$ | $A_2''$ | 8056.8704 | 3.586 | 0.414 | $4pE'$ | $+$ |
| $24d$ | 29369 | $(3,0,0)\{2,0^0\}$ | $A_2'$ | 6754.9818 | 3.999 | 0.001 | $4dE''$ | $-$ |
| | | $(1,1,3)\{0,2^2\}$ | $A_2''$ | 4994.8507 | 4.638 | 0.362 | $5pE'$ | $+$ |
| $44d$ | 29505 | $(2,2,3)\{0,3^1\}$ | $A_2'$ | 7122.6770 | 3.933 | 0.067 | $4dE'$ | $-$ |
| | | $(2,1,3)\{0,2^2\}$ | $A_2''$ | 5181.2147 | 4.615 | 0.385 | $5pE'$ | $+$ |
| | | $(1,1,0)\{0,3^1\}$ | $A_2''$ | 7083.2190 | 3.944 | 0.056 | $4pA_2''$ | $-$ |
| | | $(1,1,0)\{2,1^1\}$ | $A_2''$ | 8573.4696 | 3.584 | 0.416 | $4pE'$ | $+$ |
| $61d$ | 29531 | $(2,2,3)\{0,3^1\}$ | $A_2'$ | 7122.6770 | 3.940 | 0.060 | $4dE'$ | $-$ |
| | | $(2,1,3)\{0,2^2\}$ | $A_2''$ | 5181.2147 | 4.627 | 0.373 | $5pE'$ | $+$ |
| | | $(1,1,0)\{0,3^1\}$ | $A_2''$ | 7083.2190 | 3.951 | 0.049 | $4pA_2''$ | $-$ |
| | | $(1,1,0)\{2,1^1\}$ | $A_2''$ | 8573.4696 | 3.589 | 0.411 | $4pE'$ | $+$ |

[a]Center of the perturbed region in $cm^{-1}$.

[b]$H_3^+$ core state labeled by $(N^+,K^+,G)\{\nu_1,\nu_2^{l_2}\}$.

[c]Energies of $H_3^+$ in $cm^{-1}$ from Ref. [35] relative to the $N^+=0$ ground state. The energy of the lowest *ortho* state $(1,0,0)\{0,0^0\}$ is 86.9683 $cm^{-1}$.

[d]Effective principal quantum number determined from the core energy and the 29 562.15 $cm^{-1}$ energy of $H_3^+(1,0,0)\{0,0^0\}$ above $H_3$ $2p^2A_2''(N=K=0)\{0,0^0\}$.

[e]Quantum defect.

tion (DR) of $H_3^+$ with electrons. Because no curve crossings exist for electronic recombination below electron energies of $\approx 10$ eV, the main mechanism was thought to be the weak direct recombination due to nonadiabatic couplings between the continuum and the electronic ground state wave functions of $H_3$ [28]. The nonadiabatic couplings which govern the predissociation of $H_3$ Rydberg states can be extended to the continuum according to the $n^3$ scaling law. A theoretical model by Schneider et al. [28] is based on *ab initio* calculated coupling matrix elements for low principal quantum numbers scaled to the continuum and on predissociation rates calculated by solving the time-dependent Schrödinger equation of the nuclear motion in two dimensions. The predicted DR cross section $\sigma$ is structureless and shows a $1/\epsilon$ dependence on the excess energy $\epsilon$ of the incident electron. The measured absolute cross section [22,23], however, is by four orders of magnitude higher than the prediction of the theory [28]. Vibrationally highly excited low principal quantum number interlopers which increase the predissociation rate of high principal quantum number Rydberg states, such as the $4pE'$ and $5pE'$ states observed in this investigation, will have a substantial influence on the DR cross section and should be included in improved theoretical models. Doorway states above the first ionization threshold will give rise to structures in the DR cross section. To be relevant for the DR process, such interlopers must develop predissociation rates which are comparable to the autoionization rate. The results shown in Fig. 7 are examples of a whole class of states which fulfill this criterion.

## VI. SUMMARY

Surprisingly strong and irregular predissociation of laser-prepared low- as well as high-principal quantum number Rydberg states of $H_3$ is observed. We have investigated the lifetimes of $nsA_1'$ and $npE'$ states of $H_3$ with $n=3,4,5$ by measuring the linewidths of the transitions from the metastable state. Surprisingly, the lifetimes of states with $n=4,5$ are much shorter than those of the corresponding states with $n=3$. Our measurements demonstrate enhanced predissociation of $n=4,5$ states due to nonadiabatic couplings with the repulsive $2p^2E'$ ground state surface of $H_3$ induced by the rotational, and vibrational motion of the core. To gain insight into the dissociation dynamics of these states, detailed quantum-chemical *ab initio* calculations are required. The states are candidates for kinematically complete studies of the neutral products, and the measurement of final state distributions should provide additional information on the decay dynamics.

The high principal quantum number $ns$ and $nd$ states with $n \geq 13$ converging to the lowest ionization threshold of $H_3$ are observed in photodissociation. The absence of the $s$ series in field ionization indicates that the higher lying $s$ states are

subject to rapid predissociation. Both, the $ns$ and $nd$ series show pronounced modulations in the photofragment yield with principal quantum number which are explained by weak interactions with strongly predissociated doorway states. The doorways are tentatively assigned to the $4pE'$ and $5pE'$ electronic states with high core excitation in the vibrational degenerate mode. In addition, we have observed that states above the first ionic limit may be subject to predissociation with rates comparable to the autoionization rate. Such states play an important role in the dissociative recombination of slow electrons with $H_3{}^+$ and their inclusion in DR theory will explain the large discrepancy between the measured cross section and theoretical predictions for the direct process.

[1] G. Herzberg, J. Chem. Phys. **68**, 5298 (1978).

[2] I. Dabrowski and G. Herzberg, Can. J. Phys. **58**, 1238 (1980).

[3] M. C. Bordas, P. C. Cosby, and H. Helm, J. Chem. Phys. **93**, 6303 (1990).

[4] H. Helm, Phys. Rev. Lett. **56**, 42 (1986).

[5] H. Helm, Phys. Rev. A **38**, 3425 (1988).

[6] A. Dodhy, W. Ketterle, H.-P. Messmer, and H. Walther, Chem. Phys. Lett. **151**, 133 (1989).

[7] W. Ketterle, H.-P. Messmer, and H. Walther, Europhys. Lett. **8**, 333 (1989).

[8] L. Lembo, H. Helm, and D. L. Huestis, J. Chem. Phys. **90**, 5299 (1989).

[9] L. J. Lembo and H. Helm, Chem. Phys. Lett. **163**, 425 (1989).

[10] P. C. Cosby and H. Helm, Phys. Rev. Lett. **61**, 298 (1988).

[11] U. Müller and P. C. Cosby, J. Chem. Phys. **105**, 3532 (1996).

[12] U. Müller and P. C. Cosby, Phys. Rev. A **59**, 3632 (1999).

[13] U. Müller, Th. Eckert, M. Braun, and H. Helm, Phys. Rev. Lett. **83**, 2718 (1999).

[14] C. Bordas and H. Helm, Phys. Rev. A **43**, 3645 (1991).

[15] L. J. Lembo, M. C. Bordas, and H. Helm, Phys. Rev. A **42**, 6660 (1990).

[16] M. C. Bordas, L. J. Lembo, and H. Helm, Phys. Rev. A **44**, 1817 (1991).

[17] R. Reichle, I. Mistrik, U. Müller, and H. Helm, Phys. Rev. A **60**, 3929 (1999).

[18] I. Mistrik, R. Reichle, U. Müller, H. Helm, M. Jungen, and J. A. Stephens, Phys. Rev. A **61**, 033 410 (2000).

[19] J. A. Stephens and C. H. Greene, J. Chem. Phys. **102**, 1579 (1995).

[20] N. Bjerre, I. Hazell, and D. C. Lorents, Chem. Phys. Lett. **181**, 301 (1991).

[21] H. Helm, in *Dissociative Recombination: Theory, Experiment and Applications,* edited by B. R. Rowe, A. Mitchell, A. Canosa (Plenum Press, New York, 1993), pp. 145–153.

[22] M. Larsson, H. Danared, J. R. Mowat, P. Sigray, G. Sundström, L. Broström, A. Filevich, A. Källberg, S. Mannervik, K. G. Rensfelt, and S. Datz, Phys. Rev. Lett. **70**, 430 (1993).

[23] S. Datz, G. Sundström, Ch. Biedermann, L. Broström, H. Danared, S. Mannervik, J. R. Mowat, and M. Larsson, Phys. Rev. Lett. **74**, 896 (1995).

[24] T. Oka, in *Dissociative Recombination: Theory, Experiments and Applications IV*, edited by M. Larsson, J. B. A. Mitchell, and I. F. Schneider (World Scientific, Singapore, 2000), pp. 13–24.

[25] I. F. Schneider and A. E. Orel, J. Chem. Phys. **111**, 5873 (1999).

[26] Z. Amitay, A. Baer, M. Dahan, J. Levin, Z. Vager, D. Zajfman, L. Knoll, M. Lange, D. Schwalm, R. Wester, A. Wolf, I. F. Schneider, and A. Suzor-Weiner, Phys. Rev. A **60**, 3769 (1999).

[27] L. Carata, A. E. Orel, and A. Suzor-Weiner, Phys. Rev. A **59**, 2804 (1999).

[28] I. F. Schneider, M. Larsson, A. E. Orel, and A. Suzor-Weiner, in *Dissociative Recombination: Theory, Experiments and Applications IV*, (Ref. [24]), pp. 131–141.

[29] U. Müller, U. Majer, R. Reichle, and M. Braun, J. Chem. Phys. **106**, 7958 (1997).

[30] U. Müller, M. Braun, R. Reichle, and R. F. Salzgeber, J. Chem. Phys. **108**, 4478 (1998).

[31] J. T. Hougen, J. Chem. Phys. **37**, 1433 (1962).

[32] A. B. Raksit, R. F. Porter, W. P. Garver, and J. J. Leventhal, Phys. Rev. Lett. **55**, 378 (1985).

[33] R. Bruckmeier, Ch. Wunderlich, and H. Figger, Phys. Rev. Lett. **72**, 2550 (1994); Phys. Rev. A **52**, 334 (1995).

[34] The residual saturation broadening was corrected according to Eq. (4) in Ref. [9]. For a 15 ns laser pulse and a peak maximum of 30% of the saturation, the true linewidth $\gamma_t$ is related to the fitted linewidth $\gamma_f$ by $\gamma_t = 0.91(\gamma_f - \gamma_l)$.

[35] O. L. Polyansky and J. Tennyson, J. Chem. Phys. **110**, 5056 (1999).

[36] H. F. King and K. Morokuma, J. Chem. Phys. **71**, 3213 (1979).

[37] A. E. Orel and K. C. Kulander, Phys. Rev. Lett. **71**, 4315 (1993); A. E. Orel and K. C. Kulander, J. Chem. Phys. **91**, 6086 (1989); J. L. Krause, K. C. Kulander, J. C. Light, and A. E. Orel, *ibid.* **96**, 4283 (1992); J. L. Krause, A. E. Orel, B. H. Lengsfield, and K. C. Kulander, in *Time-Dependent Quantum Molecular Dynamics*, edited by J. Broeckhove and L. Lathouwers (Plenum, New York, 1992), p. 131.

[38] I. D. Petsalakis, G. Theodorakopoulos, and J. S. Wright, J. Chem. Phys. **89**, 6850 (1988).

[39] H. Figger, W. Ketterle, and H. Walther, Z. Phys. D: At., Mol. Clusters **13**, 129 (1989).